Multidisciplinary ⋮ Rapid Review ⋮ Open Access Journal

Date of publication xxxx 00, 0000, date of current version xxxx 00, 0000.

*Digital Object Identifier 10.1109/ACCESS.2017Doi Number*

# Change detection in multitemporal monitoring images under low illumination

**YONG ZHU[1,2], ZHENHONG JIA[1,2], JIE YANG [3], AND NIKOLA K. KASABOV [4], (Fellow, IEEE)**

[1]College of Information Science and Engineering, Xinjiang University, Urumqi 830046, China

[2]Key Laboratory of Signal Detection and Processing, Xinjiang Uygur Autonomous Region, Xinjiang University, Urumqi 830046, China

[3]Institute of Image Processing and Pattern Recognition, Shanghai Jiao Tong University, Shanghai 200400, China

[4]Knowledge Engineering and Discovery Research Institute, Auckland University of Technology, Auckland 1020, New Zealand

Corresponding author: Zhenhong Jia (jzhh9009@sohu.com)

This work was supported by the National Science Foundation of China under Grant U1803261 and the International Science and Technology Cooperation Project of the Ministry of Education of the People's Republic of China under Grant DICE 2016–2196.

**ABSTRACT** Video surveillance may involve the simultaneous monitoring of a large number of areas. Real-time automatic change detection of a monitoring area (such as involving the movement of people or vehicles) can reduce risks incurred in negligent manual observation. However, the low signal-to-noise ratio (SNR) of dark environments can significantly corrupt camera images, making it difficult for machine learning surveillance systems to detect small changes in monitored images. In addition, in the absence of changes between two multitemporal monitoring images, sensor noise can lead to false alarms. The objective of this paper is to reduce the effect of sensor noise on change detection of monitored images and the run time of change detection algorithms. For these purposes, we proposed a novel multitemporal monitoring image change detection algorithm based on morphological structure filtering and normalized fusion difference image. First, the random noise in two surveillance images was removed using a multidirectional weighted multiscale series of a morphological filter. Next, two difference images were obtained by using the compression log-ratio operator and the mean ratio operator, and a fusion difference image was obtained by equal-weight fusion of the two difference images. Then, the sigmoid function was used to compress the fusion difference map to obtain a normalized fusion difference image, and a median filter was used to obtain a final difference image. Finally, the k-means clustering algorithm was utilized to obtain the change detection results. The experimental results demonstrate that the proposed method can accurately detect changes in a night monitoring scene in real time. Subjective and objective evaluation of the experimental results demonstrate that the proposed method is superior to reference algorithms in terms of change detection accuracy, time and robustness.

**INDEX TERMS** change detection; morphological structure filtering; normalized fusion difference map; low illumination monitoring image

## I. INTRODUCTION

Surveillance cameras are widely used in the field of public safety. Special situations may require the simultaneous monitoring of dozens or hundreds of areas. Guards must watch displays of different areas on multiple monitors at the same time. For various reasons, abnormal situations in image may not be noticed in a timely manner. Security personnel could be replaced by applying change detection methods to video images. Generally, video image change detection method is to detect the change of the same scene image at different times. However, there are some difficulties in practical applications. A detection algorithm should be able to detect changes in a monitoring scene accurately and quickly for low-illumination monitoring areas (at night, for example) and very slow-moving objects. Although infrared cameras produce superior image quality under low illumination, ordinary cameras are still typically used for cost considerations. However, video images captured by ordinary cameras in low-illumination environments [1, 2] have low signal-to-noise ratios (SNRs). Thus, image change detection must be investigated under noise interference.

Although there is no research report based on the change

This article has been accepted for publication in a future issue of this journal, but has not been fully edited. Content may change prior to final publication. Citation information: DOI 10.1109/ACCESS.2020.3008262, IEEE Access



detection of two multitemporal monitoring images, numerous studies have been carried out on change detection of remote sensing images under noise interference. In recent years, several methods have been developed to reduce the noise in change detection of remote sensing images, such as in [3] and [4]. To better identify the changes between two multitemporal remote sensing images, various methods have been developed to suppress the influence of noise between two multitemporal remote sensing images: the mean ratio difference image [5], the neighborhood ratio difference image [6], the log-ratio difference image [7], and the fusion difference image [8]. However, these methods cannot completely remove the effect of noise in a remote sensing image during change detection. Thus, other methods were required to perform multiscale decomposition of the difference image generated by the two multitemporal images: the nonsubsampled contourlet transform (NSCT) [9], the discrete wavelet transform(DWT) [10], the nonsubsampled shearlet transform (NSST) [11]. The difference image was decomposed in the transform domain for denoising, after which the change region was obtained by clustering the difference image. Although these methods improved the change detection accuracy of remote sensing images, they also increased the running time of the change detection algorithm. Other change detection methods, such as the principal component analysis (PCA) [12], the Gram–Schmidt transformation [13] and the scale-invariant feature transformation (SIFT) [14], mapped the original image into the feature space to label the changed areas. The evolution of artificial intelligence has resulted in the development of deep-learning-based change detection methods for multitemporal remote sensing images: the self-paced learning method [15], the principal component analysis network (PCANET) [16], the convolutional wavelet neural network (CWNN) [17], etc. The pixels in the difference image were pre-classified and used to train the network. Saliency extraction has also recently been applied in change detection [18, 19].

Most current change detection algorithms successfully suppress the influence of speckle noise on change detection of a remote sensing image but do not significantly affect sensor noise in a low-illumination monitoring image. In the past decades, plenty of methods were proposed to denoise images, such as Markov random field [20]， nonlocal self-similarity [21, 22], and sparse representation [23-25]. Most of them were built on a simple noise model, i.e., the independent and identically distributed additive white Gaussion noise (AWGN). However, in the actual low illuminance monitoring image, there are usually complex random noise [1, 2]. In order to improve the accuracy of monitoring image change detection under the condition of low illumination. In this paper, a multidirectional weighted multiscale series morphological filter is proposed to suppress the interference of random noise on change detection. Then, the residual noise is further removed by using the fusion log-ratio and mean ratio difference images, while the details of the change area are retained.

On the other hand, all current multitemporal image change detection methods use scene changes reflected by multitemporal images to detect the differences between images. Scene changes increase the difference between changed and unchanged regions, which can suppress the influence of the difference in the sensor noise between images during change detection. Here, we report for the first time that for unchanging scenes in actual low-illumination video monitoring, many change detection algorithms often identify differences between multitemporal monitoring images that result in false alarms. We attribute this false detection to noise from the camera image sensor. Evidence is provided in Figures 1 and 2 for the change detection process for changing and unchanging scenes between two multitemporal monitoring images, respectively. Additional evidence is provided by change detection results for two datasets, experimental data 5 and experimental data 6, in part III of this paper.

The discussion above shows that existing multitemporal image change detection algorithms cannot perform accurate change detection for monitored images under low illumination. False alarms are easily triggered for unchanging scenes in video monitoring. In order to accurately detect in real time, the changes in the multitemporal monitoring image under the condition of low illumination, and avoid false alarm when the scene reflected by the monitoring video does not change, we proposed a change detection algorithm for multitemporal surveillance images under low illumination conditions. Compared with the previous multitemporal image change detection work, our method offers the following contributions.

(1) Current multitemporal image change detection schemes use a detection algorithm to determine differences between images at different times. We report for the first time that in actual low illumination video monitoring, many change detection algorithms often detect differences between multitemporal monitoring images for unchanging scenes, resulting in false alarms. We attribute this false detection to the noise produced by the camera image sensor.

(2) Most current change detection algorithms have successfully suppressed the influence of the speckle noise on the change detection of a remote sensing image. However, the sensor noise in a low-illumination monitoring image is not affected. We proposed a novel change detection method based on a multidirectional weighted multiscale series structure filter and normalized fusion difference image. This method successfully removes the interference of sensor noise on change

This article has been accepted for publication in a future issue of this journal, but has not been fully edited. Content may change prior to final publication. Citation information: DOI 10.1109/ACCESS.2020.3008262, IEEE Access



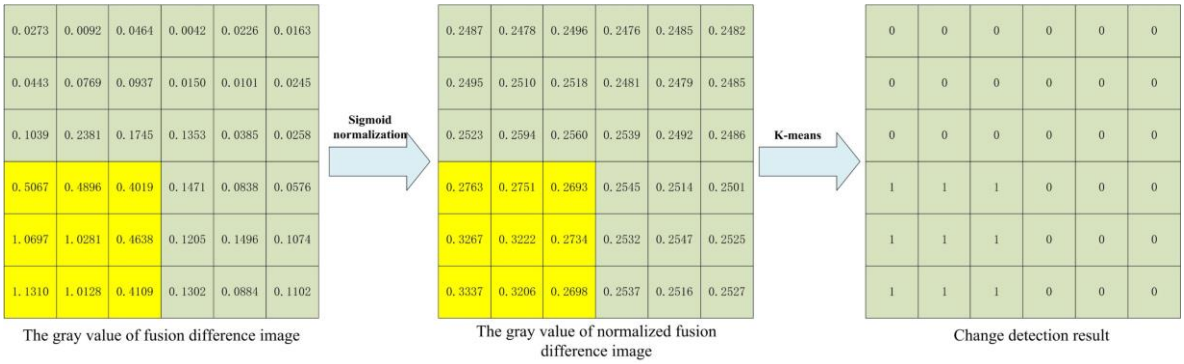


**FIGURE 1. The change detection process is shown for a partial gray value for a scene change reflected by two multitemporal monitoring images. The difference between the changed and unchanged areas of the images suppresses the corresponding difference in the sensor noise and improves subsequent clustering performance. Here, the yellow area represents the pixel value of the changed area, and '1' and '0' represent the changed and unchanged pixels, respectively.**

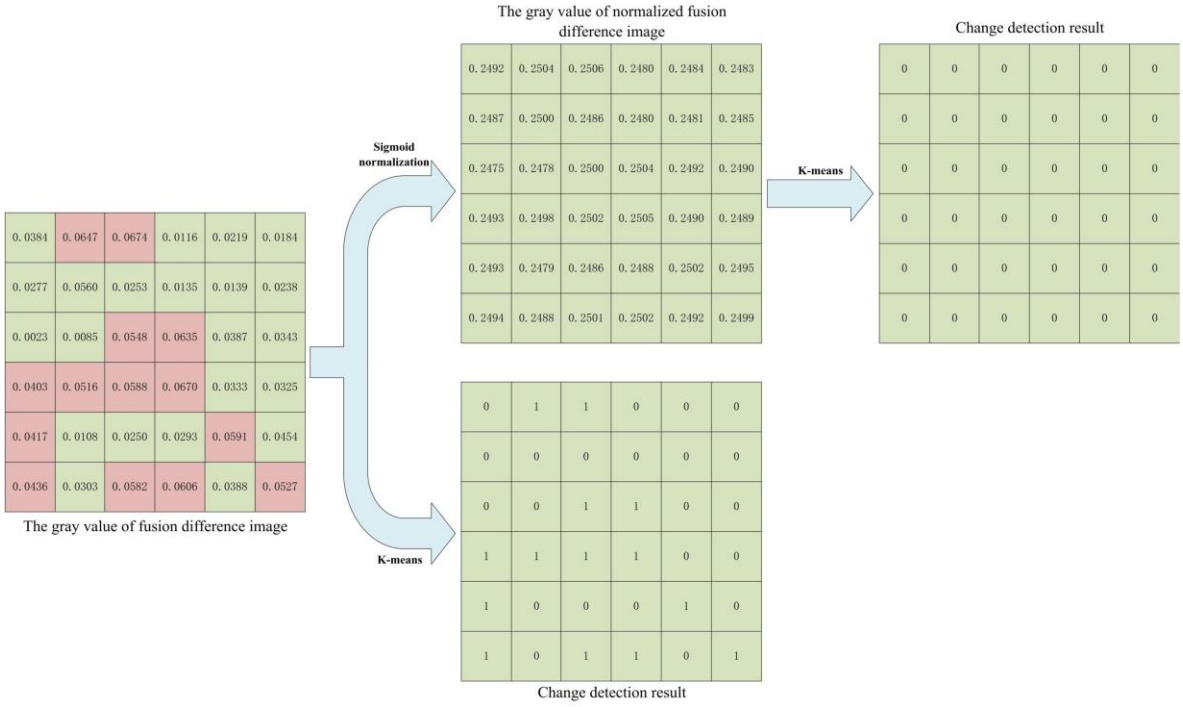


**FIGURE 2. The change detection process is shown for a partial gray value for an unchanged scene reflected by two multitemporal monitoring images. The absence of a scene change highlights the difference in the sensor noise between the images, resulting in false detection. However, the normalization operation of a sigmoid function can suppress the difference in sensor noise between the images to improve subsequent clustering performance. Here, the red area represents pixels with large differences in the sensor noise between multitemporal monitoring images, and '1' represents unchanged pixels that are misclassified as changed pixels.**

detection, while retaining the details of the change area. Compared with other reference methods, the accuracy of change detection is improved and the running time of change detection is reduced. Especially when the scene reflected by the multitemporal images does not change, the occurrence of false alarm is avoided.

The remainder of this paper is organized as follows. Section II will give the proposed algorithm framework and introduce the method in detail. Section III will introduce the experimental data of the different scenes, show the experimental results, and verify the feasibility of the method. Finally, the conclusions are drawn in Section IV.

## II. PROPOSED METHOD

Mathematical morphology is characterized by a simple structure and convenient calculations. The edges and details of the images obtained by morphology filters are well preserved. Mathematical morphology is widely used in image denoising [26], synthetic aperture radar (SAR) image change detection [27], image fusion [28] and color image segmentation [29]. In [27], Liu used mathematical morphology filtering to remove the speckle noise in a SAR image, thereby improving the accuracy and reducing the run time of change detection. In a low illumination monitoring scene, the image captured by the camera will be seriously affected by the sensor noise due to the lack of light. To

This article has been accepted for publication in a future issue of this journal, but has not been fully edited. Content may change prior to final publication. Citation information: DOI 10.1109/ACCESS.2020.3008262, IEEE Access



reduce the impact of the sensor noise on the change detection in the multitemporal monitoring image and reduce the running time, in this paper, an unsupervised change detection algorithm based on morphological structure filtering and normalized fusion difference image is proposed. Let $X_1 = \{X_1(i,j)|1 < i < h, 1 < j < w\}$ and $X_2 = \{X_2(i,j)|1 < i < h, 1 < j < w\}$ be two multitemporal monitoring images of the same scene at different times. The two images have the same width $w$ and height $h$. The change detection result is denoted by $\omega = \{\omega_c, \omega_u\}$, where $\omega_c$ and $\omega_u$ represent changed and unchanged pixels, respectively. Figure 3 is a flow chart showing the four main steps of the algorithm: 1) the images are denoised using multidirectional weighted multiscale series morphological filtering; 2) two difference images are obtained by using the compression log-ratio operator and the mean ratio operator, and a fusion difference image is obtained by equal weight fusion of the two difference images; 3) the sigmoid function is used to normalize the fusion difference image, and a median filter is used to obtain the final difference image; 4) use the k-means clustering algorithm, which does not require any distribution assumption, to find the changed area and unchanged area.

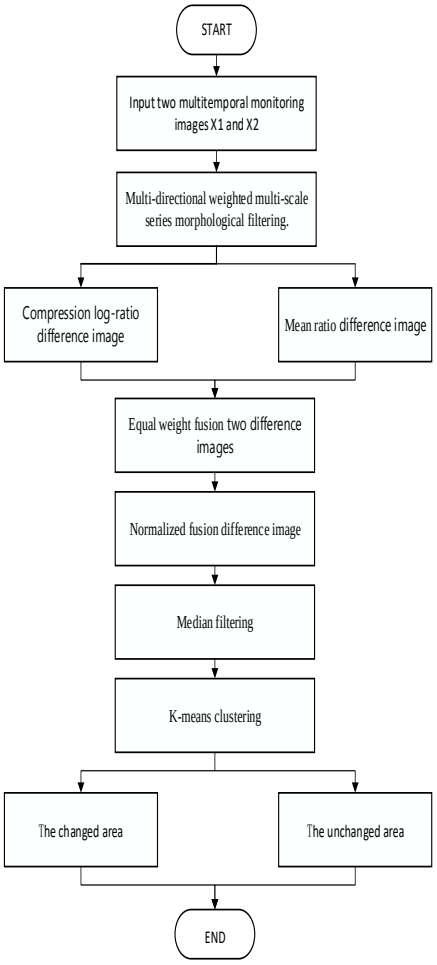


**FIGURE 3. Algorithm framework for change detection.**

### A. MULTIDIRECTION WEIGHTED MULTISCALE SERIES STRUCTURE FILTERING

Mathematical morphology operations include two sets in image processing: an image pixel set and a small set or image of the structured elements (SEs). Dilation, erosion, opening and closing are four basic operations in mathematical morphology [30]. Using a combination of dilation and erosion can yield all the morphological filters [31]. The dilation operation and erosion operation are defined as follows, respectively.

$$G \oplus S(x,y) = \max_{(x',y') \in s} \{G(x-x', y-y') + S(x',y')\} \quad (1)$$

$$G \Theta S(x,y) = \max_{(x',y') \in s} \{G(x+x', y+y') - S(x',y')\} \quad (2)$$

where G represents a gray image, the value of a pixel $(x, y)$ in G is represented by $G(x, y)$ ; and S represents the SE, the value of a pixel $(x', y')$ in S is represented by $S(x', y')$. Dilating an image is the same as finding the local maximum and will increase the highlighted area in the image. The erosion operation can eliminate the boundary points of the objects, which can remove objects smaller than the structural elements.

Dilation and erosion processes can be implemented to obtain the open operation and the close operation, which are defined consecutively below:

$$G \circ S = (G \Theta S) \oplus S \quad (3)$$

$$G \bullet S = (G \oplus S) \Theta S \quad (4)$$

The open operation is often used to remove small bright details that are smaller than SEs, and the close operation removes small dark details. Alternately, the open and close operations can be used to remove the small noise components [32]. The morphology filter is given as follows.

$$(G \circ S) \bullet S = \{(G \Theta S) \oplus S\} \bullet S \quad (5)$$

To eliminate random noise in two multitemporal monitoring images, the morphological structure filter in formula (5) is used to conduct multidirectional weighted multiscale series filtering on the two input images. A linear element is selected for the SEs, which is defined using two lengths (a and b) and four angles (0°, 45°, 90° and 135°). Four types of structure groups are considered: $SE_1$, $SE_2$, $SE_3$ and $SE_4$. The input image is filtered in series by using structure groups with different angles to obtain four filtered images. These images are weighted and summed to obtain a smooth image after removal of the random noise. Let $X = \{X(i,j)|1 < i < h, 1 < j < w\}$ be the input image, where $h$ and $w$ represent the height and width of the input image, respectively. Therefore, the input gray image X is filtered by the multidirectional weighted multiscale cascade structure to obtain a smooth image Y, which is defined as follows:

$$Y = \sum_{i=1}^{4} W_i \times X_i \quad (6)$$

This article has been accepted for publication in a future issue of this journal, but has not been fully edited. Content may change prior to final publication. Citation information: DOI 10.1109/ACCESS.2020.3008262, IEEE Access



where $X_1$, $X_2$, $X_3$ and $X_4$ are the images filtered by the input image X through $SE_1$, $SE_2$, $SE_3$ and $SE_4$, respectively. Here, $W_1$, $W_2$, $W_3$ and $W_4$ are the number of times that $SE_1$, $SE_2$, $SE_3$ and $SE_4$ insert images divided by the total number of insertions, respectively:

$$W_i = (a_i + b_i) \div sum \tag{7}$$

where $a_i$ and $b_i$ are the number of times that filters of sizes a and b in $SE_i$ are inserted into the image (where $i$ = 1, 2, 3 and 4); sum is the total number of insertions of $SE_1$, $SE_2$, $SE_3$ and $SE_4$. The $a_i$ and $b_i$ values are calculated as follows:

$$a_1 = (w - a + 1) \times h \tag{8}$$

$$b_1 = (w - b + 1) \times h \tag{9}$$

$$a_2 = (h - a + 1) \times (w - a + 1) \tag{10}$$

$$b_2 = (h - b + 1) \times (w - b + 1) \tag{11}$$

$$a_3 = (h - a + 1) \times w \tag{12}$$

$$b_3 = (h - b + 1) \times w \tag{13}$$

$$a_4 = a_2 \tag{14}$$

$$b_4 = b_2 \tag{15}$$

$$sum = \sum_{i=1}^{4} (a_i + b_i) \tag{16}$$

where $h$ represents the height of the input image X, and $w$ represents the width of the input image X.

### B. GENERATION OF DIFFERENCE IMAGE

The denoising of X1 and X2 by multidirectional weighted multiscale series morphological filtering produces the images Y1 and Y2. $F_L$ and $F_D$ are generated by the compressed log-ratio operator and the mean ratio operator as follows:

$$F_L = \alpha * \left| \mathrm{lb} \frac{Y_1(i,j) + \beta}{Y_2(i,j) + \beta} \right| \tag{17}$$

$$F_D = 1 - \min\left( \frac{\mu_1(i,j)}{\mu_2(i,j)}, \frac{\mu_2(i,j)}{\mu_1(i,j)} \right) \tag{18}$$

where lb represents a logarithmic transformation; and $Y_1(i,j) + \beta$ and $Y_2(i,j) + \beta$ are used instead of $Y_1(i,j)$ and $Y_2(i,j)$, respectively, to prevent cases in which $Y_1(i,j)$ or $Y_2(i,j)$ have zero pixel values. Here, α is to compress the difference between the gray values of the log-ratio difference image and to better suppress the sensor noise. In this paper, α is taken as 0.5. After using the compressed log-ratio operator, we normalize $F_L$ to the range [0, 4]. Here, $\mu_1(i,j)$ and $\mu_2(i,j)$ are the mean values of all the pixels in a 3×3 neighborhood of pixel $(i,j)$ in Y1 and Y2, respectively.

The quality of the difference image determines the performance of the change detection results. The advantage of the log-ratio operate is the ability to convert multiplicative coherent noise to additive noise, and the background information of the difference image obtained by the log-ratio operate is relatively flat. The disadvantages are that the log-ratio operate compresses the variation range of the difference image, and has the characteristics of enhancing the low intensity pixels to weaken the high intensity pixels, and cannot reflect the real change trends to the maximum extent, which may lead to the loss of the changed area. However, the mean ratio operate does not have such problems. The mean ratio difference image can effectively enhance the contour of the change area and changes in a small area, and can also prevent the loss of change information. Therefore, the fusion of log-ratio and mean ratio difference images can effectively remove the noise, while retaining the change area. Some scholars have improved the accuracy of change detection by fusing different difference images in transform domain [33, 34]. However, this approach is relatively complicated to implement and can increase the run time. Inspired by [11], we use simple equal-weight fusion to compress the log-ratio and mean ratio difference images, thereby improving the quality of the difference image and the change detection accuracy while reducing the run time. A simple equal weight fusion difference image R can be obtained by the following formula (19):

$$R(i,j) = 0.5F_L(i,j) + 0.5F_D(i,j) \tag{19}$$

### C. NORMALIZED FUSION DIFFERENCE IMAGE

As previously explained, an image change detection algorithm identifies the change area between two images of the same scene at different times. Changes in multitemporal images increase the difference between changed and unchanged areas. This difference suppresses noise interference in change detection to some extent. However, in the actual low illumination video monitoring, the scene reflected by the video does not change. In this case, the difference in the sensor noise between the two multitemporal images interferes with image change detection. Thus, the absence of change scenes reflected by multitemporal images highlights differences in the sensor noise. In this paper, we use the sigmoid function to normalize the fusion difference image to the range [0.2, 1.2]. Our objective is to compress the difference between unchanged and changed pixels caused by sensor noise. This approach can suppress noise and improve subsequent clustering performance to some extent. The normalized fusion difference image can be obtained by formula (20).

$$ZR(i,j) = \frac{1}{1 + e^{-(R(i,j)-3)}} + 0.2 \tag{20}$$

### D. K-MEANS CLUSTERING ALGORITHM

Extraction of the change region from the final fusion difference image divides the final difference image into changed and unchanged areas. Common segmentation algorithms that can be used for this purpose include threshold algorithms [35] and clustering algorithms [36]. Threshold

This article has been accepted for publication in a future issue of this journal, but has not been fully edited. Content may change prior to final publication. Citation information: DOI 10.1109/ACCESS.2020.3008262, IEEE Access



algorithms must establish a statistical model for the difference image. The complexity of the statistical features makes it difficult to build an accurate model. Unlike the threshold algorithm, clustering algorithms effectively complete image classification without considering image statistical characteristics. The k-means clustering algorithm offers the advantages of a short calculation time and simple operation, effectively reducing the run time of the change detection algorithm [27]. In this paper, we use the k-means algorithm to cluster the obtained difference image.

According to the Euclidean distance based on formula (21), we can acquire the change detection image C. The following process is performed:

$$C(i,j)=\begin{cases}1, & \left|ZR'(i,j)-V_c\right|\le\left|ZR'(i,j)-V_u\right| \\ 0, & \text{otherwise}\end{cases} \tag{21}$$

where $V_c$ represents the mean feature vectors for the changed class and $V_u$ represents the mean feature vectors for the unchanged class, and $V_c$ and $V_u$ can be obtained by random initialization. Here, '1' and '0' represent the changed pixel and the unchanged pixel, respectively.

## III. EXPERIMENTAL ANALYSIS

To verify the superiority of the proposed method, image data of different scenes were selected to perform experiments. Subjective and objective indicators were used to compare the detection results obtained using the proposed method and five other methods: NSST [11], PCA-K-means [12], PCANET [16], CWNN [17] and NR-ELM [6]. The experimental environment includes an Intel Core i7-7700@3.60 GHz processor with 8 GB of memory, and the software used was MATLAB2016 (64 bit). The objective indicators analysis of the change detection results is set as follows: the false negatives (*FN*) (changed pixels that are undetected) and the false positives (*FP*) (unchanged pixels wrongly detected as changed) should be calculated. The overall error (*OE*) is the sum of *FN* and *FP* [37]. The percentage correct classification (*PCC*) and the run time (T). In this paper, we study the subtle change of multitemporal monitoring image under low illumination. Most of the pixels in the multitemporal monitoring image are unchangeable, which will lead to the imbalance of positive and negative sample distribution. Therefore, *PCC* cannot fully represent the change detection effect of various methods. *Kappa* coefficient and *F1-score* are two better evaluation metrics for change detection. The *Kappa* statistic is a measure of the accuracy or agreement based on the difference between the error matrix and the chance agreement [38]. And *F1-score* is the harmonic average of precision and recall. We calculate the *F1-score* as follows:

$$F1-score=\frac{2*TP}{2*TP+FN+FP} \tag{22}$$

where *TP* is short for true positives, which is the number of pixels that are detected as in a changed area in both the reference image and the result. *TN* is short for true negatives, which is the number of pixels that are detected as in an unchanged area in both the reference image and the result.

### A. COMPARATIVE ACCURACY ANALYSIS OF CHANGE DETECTION METHODS

To verify the accuracy of the proposed method, three groups of multitemporal image data of different scenes were selected to perform experiments. Subjective and objective indicators were used to compare the detection results obtained using different methods.

The first set of multitemporal monitoring images is shown in Figure 4 (a) and (b), where the camera was positioned to take two images of the same scene one second apart. In the two images, only the position of the black car has changed slightly. The two images are 256 × 256 pixels in size. Figure 4 (c) shows the change reference image. The white pixels represent the changed area in Figure 4 (c).

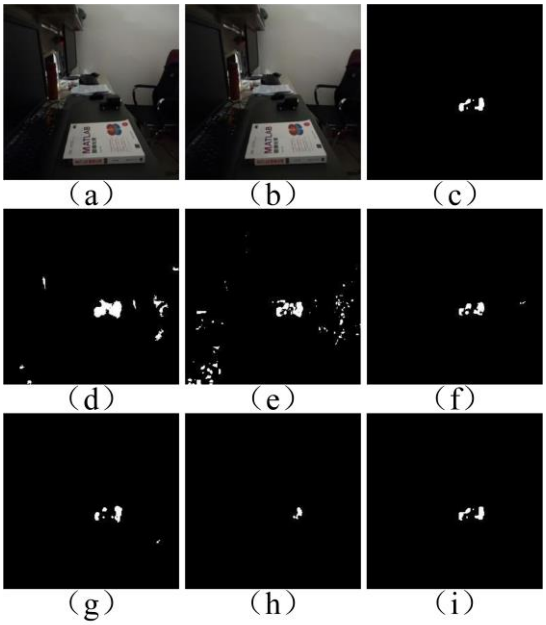


**FIGURE 4. Change detection results of experiment data 1: (a) Original image, (b) Image after change, (c) The reference image, (d) PCANET, (e) NSST, (f) NR-ELM, (g) PCA-K-means, (h) CWNN, (i) Proposed**

TABLE I
PERFORMANCE MEASURES FOR THE EXPERIMENT DATA 1

| Dataset | Method | FN | FP | OE | PCC | Kappa | F1-score | T(s) |
|---|---|---|---|---|---|---|---|---|
| Data1 | PCANET | 0 | 757 | 757 | 0.9884 | 0.4282 | 0.4321 | 959 |
| | NSST | 12 | 825 | 837 | 0.9872 | 0.3871 | 0.3974 | 1.813 |
| | NR_ELM | 44 | 83 | 127 | 0.9981 | 0.7925 | 0.7935 | 8.156 |
| | PCA_KMEANS | 67 | 90 | 157 | 0.9976 | 0.7367 | 0.7379 | **0.4406** |
| | CWNN | 189 | 0 | 189 | 0.9971 | 0..5105 | 0.5116 | 11.687 |
| | PROPOSED | 10 | 17 | 27 | **0.9996** | **0.9535** | **0.9537** | 0.5709 |

The experimental data 1 was used to test the accuracy of the proposed change detection method and to compare it with

This article has been accepted for publication in a future issue of this journal, but has not been fully edited. Content may change prior to final publication. Citation information: DOI 10.1109/ACCESS.2020.3008262, IEEE Access



the currently in use five other methods. The experimental results are shown in Figure 4. Compared with other algorithms, the image generated by our proposed method is closer to the reference image. This result is obtained because of the considerable sensor noise in the two multitemporal monitoring images taken by the camera in the absence of light. Sensor noise typically includes random and coherent noise. In the proposed algorithm, the multidirectional weighted multiscale series structure filter removes the random noise, and the fused difference image is compressed to remove the coherent noise. Figure 4 (d) and (e) show that the change detection results of PCANET and NSST generate false alarm due to the presence of random noise; Figure 4 (f), (g) and (h) show that the change detection results of NR-ELM, PCA-K-means and CWNN reduce the noise but lose the details of the change area. In Table I, the performances of the six methods are given quantitatively. Compared with PCANET, NSST, NR-ELM and CWNN (we only calculated the test time of the CWNN algorithm, and the training time was approximately 550 seconds), our proposed method has better performance based on the *OE*, *PCC*, *Kappa* coefficients and *F1-score* and requires less time. Although the time of the PCA-K-means algorithm is shorter than that of our algorithm, the *OE*, *PCC*, *Kappa* coefficients and *F1-score* of our algorithm are obviously better than those of PCA-K-means.

A second set of multitemporal monitoring images of indoor scenes with an intrusion scenario was considered. The camera was positioned to take the original image and the image changed by the intrusion, as shown in Figure 5 (a) and (b), respectively. The two images are 256 × 256 pixels in size. Figure 5 (c) shows the change reference image.

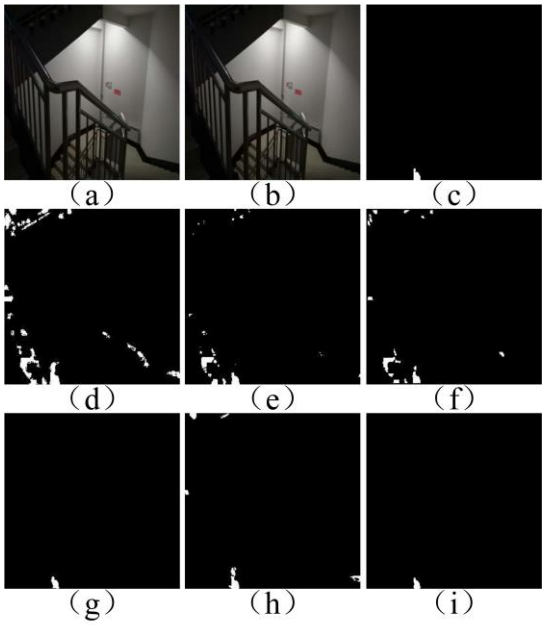


**FIGURE 5. Change detection results of experiment data 2: (a) Original image, (b) Image after change, (c) The reference image, (d) PCANET, (e) NSST, (f) NR-ELM, (g) PCA-K-means, (h) CWNN, (i) Proposed**

For experimental data 2, Figure 5 shows the final change detection results obtained using the proposed method and five comparative methods. PCANET and NR-ELM perform relatively poorly, as evidenced by many white spots in the corresponding change detection results. In Figure 5 (e) and (h), the final change image obtained by the NSST and CWNN methods results in many false alarms from random noise. As shown in Figure 5, the proposed method and PCA-K-means complete the change detection task well. However, looking at Figure 5 (g), we found that PCA-K-means lost some details in the detected changed area. The quantitative analysis in Table II confirms this result. The proposed method has an *FN* of 11, which is slightly lower than that of PCA-K-means. The proposed method takes 0.04 seconds longer than PCA-K-means but has the best *OE*, *PCC*, *Kappa* coefficients and *F1-score*. In addition, our method has another advantage in that it can result in lower *FP*.

TABLE II
PERFORMANCE MEASURES FOR THE EXPERIMENT DATA 2

| Dataset | Method | FN | FP | OE | PCC | Kappa | F1-score | T(s) |
|---|---|---|---|---|---|---|---|---|
| Data2 | PCANET | 0 | 1913 | 1913 | 0.9708 | 0.1092 | 0.1123 | 1288 |
| | NSST | 0 | 500 | 500 | 0.9924 | 0.3197 | 0.3261 | 1.675 |
| | NR_ELM | 20 | 561 | 581 | 0.9911 | 0.2557 | 0.2580 | 7.978 |
| | PCA_KMEANS | 19 | 24 | 43 | 0.9993 | 0.8256 | 0.8259 | **0.4361** |
| | CWNN | 0 | 308 | 308 | 0.9953 | 0.4384 | 0.4400 | 12.014 |
| | PROPOSED | 11 | 2 | 13 | **0.9998** | **0.9441** | **0.9442** | 0.4781 |

A third set of multitemporal monitoring images for an outdoor abnormal change scene was considered. Figure 6 (a) and (b) are two multitemporal monitoring images of the same scene at different times. The two images are 256 × 256 pixels in size. Figure 6 (c) shows the change reference image.

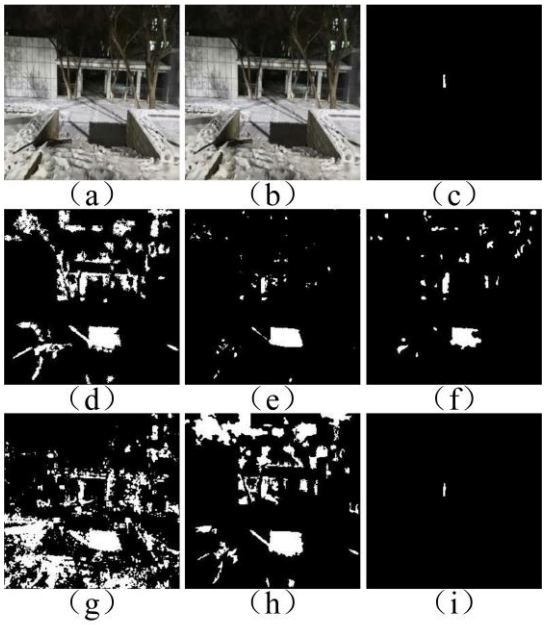


**FIGURE 6. Change detection results of experiment data 3: (a) Original image, (b) Image after change, (c) The reference image, (d) PCANET, (e) NSST, (f) NR-ELM, (g) PCA-K-means, (h) CWNN, (i) Proposed**

This article has been accepted for publication in a future issue of this journal, but has not been fully edited. Content may change prior to final publication. Citation information: DOI 10.1109/ACCESS.2020.3008262, IEEE Access



Experimental data 3 is an outdoor scene, the background is more complex than the indoor scene, and the sensor noise in the two images captured by the camera has more serious interference during the change detection. As seen from Figure 6, the performance of PCA-K-means, PCANAT and CWNN is poor because of the obvious misclassification. There are many false alarms in the results of NR-ELM and NSST due to random noise. It can also be seen that (d), (e), (f), (g) and (h) present a large area of white, which occurs because the light of the same scene changes slightly at different times, resulting in a gray difference between the two images. However, our method uses the normalized fusion difference map to suppress the subtle gray differences caused by the subtle light changes. The quantitative analysis is given in Table III. The *FN* of the other methods is 0 because of their poor *FP*. In addition, the *OE*, *PCC*, *Kappa* coefficients and *F1-score* show that the proposed method outperforms the other methods. And the time required is only approximately 0.5 seconds, which meets that it meets the requirements of real-time.

TABLE III
PERFORMANCE MEASURES FOR THE EXPERIMENT DATA 3

| Dataset | Method | FN | FP | OE | PCC | Kappa | F1-score | T(s) |
|---|---|---|---|---|---|---|---|---|
| Data3 | PCANET | 0 | 7995 | 7995 | 0.8780 | 0.0132 | 0.0150 | 1240 |
| | NSST | 0 | 1796 | 1796 | 0.9726 | 0.0621 | 0.0636 | 1.645 |
| | NR_ELM | 0 | 2254 | 2254 | 0.9656 | 0.0496 | 0.0513 | 7.718 |
| | PCA_KMEANS | 0 | 13578 | 13578 | 0.7928 | 0.0071 | 0.0089 | 0.5037 |
| | CWNN | 0 | 9356 | 9356 | 0.8572 | 0.0110 | 0.0129 | 14.264 |
| | PROPOSED | 11 | 7 | 18 | **0.9997** | **0.8473** | **0.8475** | **0.4839** |

## B. ANALYSIS OF EXPERIMENTAL PARAMETERS

In the process of multidirectional weighted multiscale series morphological filtering, the sizes of the linear SEs, a and b, must be appropriately chosen to obtain accurate change detection results. Small SEs preserve detail but are susceptible to noise. Large SEs blur details while removing noise. The size of a linear SE should be larger than that of a noisy image but smaller than that of a non-noisy image. In this paper, the lengths of a and b are chosen as 3 and 5, respectively. The two types of linear SEs are connected in series. Subsequent filtering of the multitemporal monitoring images removes the influence of sensor noise on change detection, while retaining the details of the change area. Figure 10 shows the change detection results of single-scale structure filtering and multiscale series structure filtering based on experimental data 1, 2 and 3.

As shown in Figure 7, the change detection results of experimental data 1 and experimental data 2 are different after filtering at different scales. For single-scale structure filtering with a = 3, some false alarms are generated because of the incomplete removal of the random noise. This result is obtained because a small linear SE preserve the details of the change area but is easily affected by noise. For the single-scale structure filtering with b = 5, some details are lost in the detected change area. This result is obtained because a large linear SE eliminates noise but blurs details. By comparison, multiscale series structure filtering with linear SE lengths a = 3 and b = 5 improves the change detection results, by removing noise while retaining the details of the change area. For experimental data 3, the same change detection results are obtained by different scale filtering.

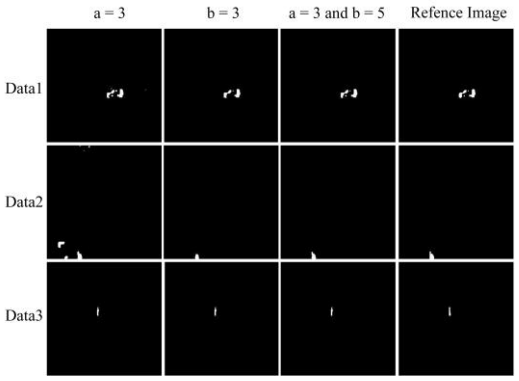


**FIGURE 7. change detection results of single-scale structure filtering and multiscale series structure filtering**

In generating a log-ratio difference image, proper selection of the parameter β is very important to obtain accurate change detection results. In this paper, β was set to 0.1, 1, 10 and 100 in the change detection experiments. The experimental results show that the best change detection results are obtained for a β of 1. Figure 8 shows the change detection results for different β values using experimental data 1 and 2. In addition, we used 50 sets of multitemporal monitoring images to experiment with using different β values. The relationship between the objective index of the average experimental results and β is shown in Table IV.

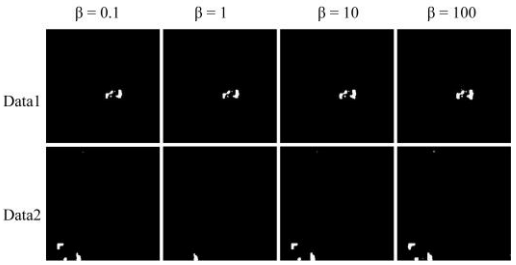


**FIGURE 8. change detection results of different parameters β based on experimental data 1 and 2**

TABLE IV
THE RELATIONSHIP BETWEEN PARAMETER $\beta$ AND OBJECTIVE INDEX

| β | $\overline{\text{OE}}$ | $\overline{\text{PCC}}$ | $\overline{\text{Kappa}}$ | $\overline{F1-score}$ |
|---|---|---|---|---|
| 0.1 | 237.1 | 0.9964 | 0.6623 | 0.6630 |
| 1 | **22** | **0.9997** | **0.9028** | **0.9030** |
| 10 | 267.1 | 0.9959 | 0.6773 | 0.6780 |
| 100 | 448 | 0.9932 | 0.5189 | 0.5202 |

## C. ARTIFICIAL IMAGE CHANGE DETECTION

Experimental data 4 consists of multitemporal monitoring images generated by manual addition of a change area.

This article has been accepted for publication in a future issue of this journal, but has not been fully edited. Content may change prior to final publication. Citation information: DOI 10.1109/ACCESS.2020.3008262, IEEE Access



Figure 9 (a) shows an image at a specific time in an outdoor scene to which a changed area is manually added to produce Figure 9 (b). The two images are 256 × 256 pixels in size. Figure 9 (c) shows the change reference image.

（a） （b） （c）

**FIGURE 9. Manually adding the changed multitemporal monitoring images data: (a): original image; (b): image after adding the change; (c) The reference image**

We investigated how the noise (random component) level affects change detection in two multitemporal monitoring images. We added random noise with a uniform distribution with a zero mean and a standard deviation δ to Figure 9 (b). Figure 10 shows the final change detection results of the proposed method and five comparative methods.

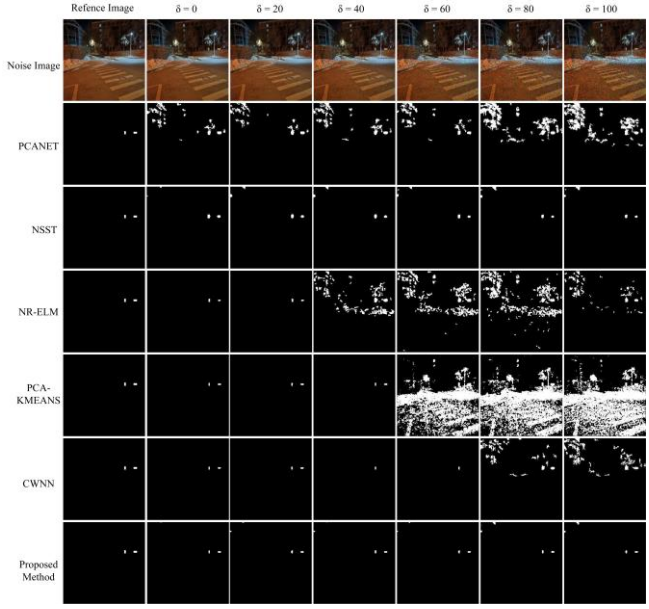


**FIGURE 10. change detection results of manually added random noise**

TABLE V
PERFORMANCE MEASURES FOR THE $\delta = 80$

| Dataset | Method | FN | FP | OE | PCC | Kappa | F1-score | T(s) |
|---|---|---|---|---|---|---|---|---|
| Data4 | PCANET | 0 | 4937 | 4937 | 0.9247 | 0.0351 | 0.0449 | 1078 |
| | NSST | 10 | 181 | 191 | 0.9971 | 0.5272 | 0.5261 | 3.217 |
| | NR_ELM | 0 | 6272 | 6272 | 0.9043 | 0.0323 | 0.0357 | 8.346 |
| | PCA_KMEANS | 0 | 26900 | 26900 | 0.5895 | 0.0050 | 0.0086 | **0.7492** |
| | CWNN | 2 | 1800 | 1802 | 0.9725 | 0.0857 | 0.1123 | 12.648 |
| | PROPOSED | 29 | 85 | **114** | **0.9983** | **0.6033** | **0.6042** | 0.7699 |

As seen from Figure 10, the proposed method and NSST obtain the best change detection results under the interference of different levels of random noise. However, with the increase of δ, there are more false alarms in the change detection results of NSST than in the change detection results of our method. The worst change detection results are obtained for PCANET, which produces many false alarms even in the absence of random noise (δ = 0). NR-ELM and PCA-K-means produce good change detection results for small δ. However, increasing δ produces significant disturbances from random noise in the NR-ELM and PCA-K-means results. For δ = 0 and δ = 20, CWNN completes the change detection task well. However, some change areas are lost for δ = 40 and δ = 60, and continuously increasing δ produces significant disturbances from random noise. Table V is a quantitative analysis of the results of the six considered methods for δ = 80. Compared to NSST, the proposed method has a lower *Kappa* coefficient but a clearly better *PCC, OE* and run time *T*. Although PCA-K-means have the shortest running time *T*, the performance based on *FP, OE, PCC, Kappa* coefficients and *F1-score* is poor. The lower *FN* of PCANET、NR-ELM、PCA-K-means and CWNN are due to their higher *FP*.

### D. ROBUSTNESS ANALYSIS OF CHANGE DETECTION METHOD

In many actual video surveillances, the scene reflected by two multitemporal monitoring images collected by the camera does not change, only the sensor noise interference image change detection. In this case, the considerable interference of sensor noise in the change detection results in a false alarm. To verify the robustness of the proposed method, experiments were conducted on experimental data 5 and 6.

The fifth set of multitemporal monitoring images selected an indoor situation without real changes. The camera was positioned to take two multitemporal images of the same scene one second apart, as shown in Figure 11 (a) and 11 (b). The two images are 256 × 256 pixels in size. Figure 11 (c) shows the change reference image. To further verify the hypothesis in Section II.C, we removed the real changes (the intrusion) from the two multitemporal images in experimental data 2 to produce experimental data 6, as shown in Figure 12 (a) and 12 (b). The pixel size of the cropped images is 193 × 193. Figure 12 (c) shows change reference image. Experimental data 5 and 6 were used to carry out the change detection experiment, and the results are shown in Figures 11 and 12 respectively.

TABLE VI
PERFORMANCE MEASURES FOR THE EXPERIMENT DATA 5

| Dataset | Method | FN | FP | OE | PCC | F1-score | T(s) |
|---|---|---|---|---|---|---|---|
| Data5 | PCANET | 0 | 7485 | 7485 | 0.8858 | 0 | 1358 |
| | NSST | 0 | 969 | 969 | 0.9852 | 0 | 2.396 |
| | NR_ELM | 0 | 1396 | 1396 | 0.9787 | 0 | 7.611 |
| | PCA_KMEANS | 0 | 16161 | 16161 | 0.7534 | 0 | 0.5006 |
| | CWNN | 0 | 2893 | 2893 | 0.9559 | 0 | 12.649 |
| | PROPOSED | 0 | 4 | **4** | **0.9999** | 0 | **0.4683** |

This article has been accepted for publication in a future issue of this journal, but has not been fully edited. Content may change prior to final publication. Citation information: DOI 10.1109/ACCESS.2020.3008262, IEEE Access



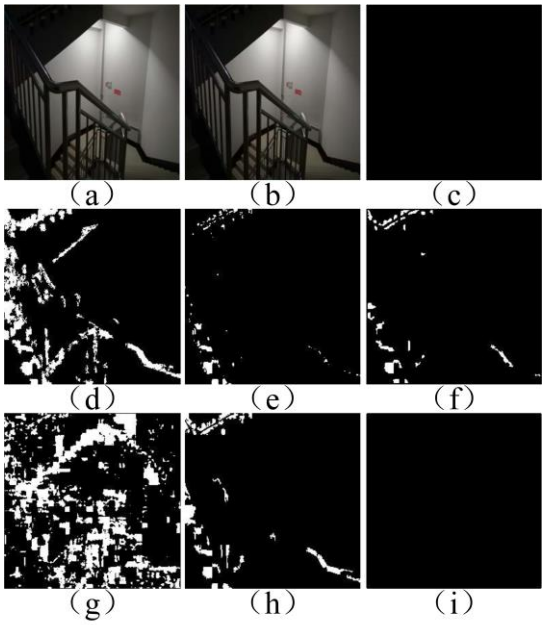


**FIGURE 11. Change detection results of experiment data 5: (a) Original image, (b) Image after 1 second, (c) The reference image, (d) PCANET, (e) NSST, (f) NR-ELM, (g) PCA-K-means, (h) CWNN, (i) Proposed**

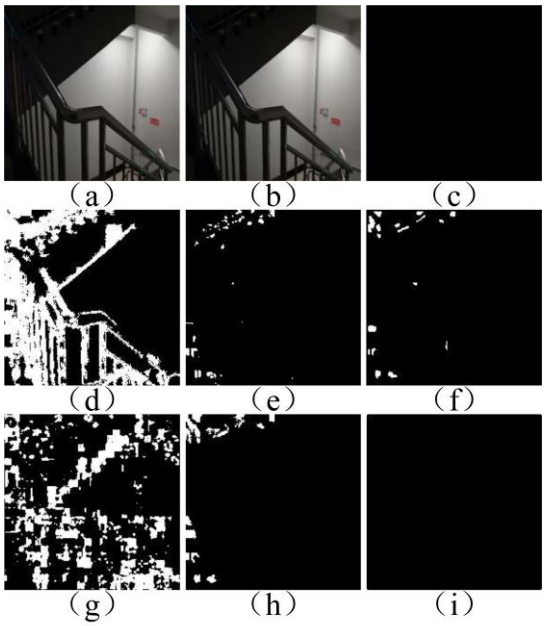


**FIGURE 12. Change detection results of experiment data 6: (a) Original image, (b) Image after change, (c) The reference image, (d) PCANET, (e) NSST, (f) NR-ELM, (g) PCA-K-means, (h) CWNN, (i) Proposed**

TABLE VII
PERFORMANCE MEASURES FOR THE EXPERIMENT DATA 6

| Dataset | Method | FN | FP | OE | PCC | F1-score | T(s) |
|---|---|---|---|---|---|---|---|
| Data6 | PCANET | 0 | 12090 | 12090 | 0.6754 | 0 | 999 |
| | NSST | 0 | 466 | 466 | 0.9875 | 0 | 1.464 |
| | NR_ELM | 0 | 507 | 507 | 0.9864 | 0 | 4.600 |
| | PCA_KMEANS | 0 | 8787 | 8787 | 0.7641 | 0 | 0.4260 |
| | CWNN | 0 | 927 | 927 | 0.9751 | 0 | 12.196 |
| | PROPOSED | 0 | 4 | 4 | **0.9999** | 0 | **0.4198** |

It can be seen from Figures 11 and 12 that when there is no change in the scene reflected by the two multitemporal monitoring images, the change detection performance of PCA-K-means, PCANET and CWNN is poor. This finding occurs because there is no real change that makes the difference between the sensor noise in the two images obvious. PCA-K-means uses the subtraction operator to obtain the difference image of two images, and then, it uses principal component analysis to obtain the feature vector of each pixel. Therefore, PCA-K-means mistakenly classifies noisy pixels into change pixels. Pre-classification by PCANET and CWNN results in noisy pixels being misclassified as change pixels. The change detection results are not accurate because the training samples are not ideal. The final image obtained by NR-ELM and NSST have many false alarms because of the existence of sensor noise. However, the proposed method uses the multidirectional weighted multiscale series filter to remove sensor noise and the sigmoid function to normalize the difference map. Thus, the interference from the difference in the sensor noise is suppressed, and the subsequent clustering performance is improved. The results of the quantitative analysis are shown in Tables VI and VII. Compared with other methods, the method based on the *OE* and *PCC* has better performance and takes less time. Since there is no change pixel in the reference image of change detection, *Kappa* coefficient is meaningless. The *F1-score* of the six algorithms is 0 because *TP* is 0.

### E. TIME COMPLEXITY OF THE PROPOSED METHOD

The running time of each change detection algorithm depends on the size of the input images，with the increase of input images size, the time requirement of each algorithm also increases. The experiment data 5 and 6 are 256 × 256 and 193 × 193 pixels in size, respectively. As shown in Tables VI and VII, as the input images size increased, the time required to run the proposed algorithm increased by 12%, compared to 36%, 64%, 65% and 18% for the PCANET, NSST, NR-ELM and PCA-K-means algorithms, respectively. The time requirement of the CWNN algorithm was increased by 4% because we only calculated the testing time of the CWNN algorithm. The small time increment of the proposed algorithm was due to its simple framework.

Next, we will talk about the time complexity of the proposed algorithm. As illustrated in Figure 3, there are a total of five steps in the proposed algorithm: multidirectional weighted multiscale series morphological filtering, fusion difference image generation, sigmoid function normalization operation, median filtering and k-means clustering. Therefore, the time complexity of the proposed algorithm is the sum of time complexities of these different processes. Let $n$ represents the total number of pixels of the input image; $l$ is the number of pixels in the largest linear SE; the window sizes of the mean ratio operator and median filtering are represented by $r_u$ and $r_m$; $k$ represents the number of cluster

This article has been accepted for publication in a future issue of this journal, but has not been fully edited. Content may change prior to final publication. Citation information: DOI 10.1109/ACCESS.2020.3008262, IEEE Access



centers and is set to 2; and $d$ is the distance calculation complexity. The k-means iteration is represented by $t$. The time complexity of each step in the proposed algorithm is shown in the following table.

TABLE VIII
TIME COMPLEXITY OF EACH PROCESS OF THE PROPOSED METHOD

| Process | Complexity | Process | Complexity |
|---|---|---|---|
| Morphological structure filtering | $O(8ln)$ | median filtering | $O({r_m}^2 n)$ |
| Generate fusion difference map | $O({r_u}^2 n)$ | K-means clustering | $O(kndt)$ |
| Sigmoid function normalization | $O(n)$ | Proposed method | $O(8ln + kndt)$ |

For the proposed morphological structure filtering method, first, the time complexity of single direction multiscale series structure filtering is $O(ln)$. Then, multiscale series structure filtering is applied to four different directions of two multitemporal images, respectively. Therefore, the time complexity of the proposed morphological structure filtering method is $O(8ln)$. Because $r_u$, $r_m$ are much smaller than $8l$ and $dt$, as shown in Table VIII, the complexity of the proposed algorithm is $O(8ln + kndt)$.

### F. ANALYSIS OF THE AVERAGE EXPERIMENTAL RESULTS

Due to the limited space of the paper, we used 50 sets of multitemporal monitoring image data to test and calculate the average results of the six algorithms discussed in the previous section. Each of the 50 sets of images includes two images taken at different times of the same scene and a manually analyzed reference detected changed area image. The test of each group of data was run 10 times to obtain the average change detection result, as shown in Table IX. These average results show that the proposed method has the best performance based on the *OE, PCC, Kappa* coefficients and *F1-score* compared with the other five methods. The proposed method outperforms the PCANET、NR-ELM、NSST and CWNN methods in terms of the detection time.

In addition, we used 100 groups of artificially generated image data to test the effect of different random noise levels on image change detection. Figures 13 and 14 show the relationship between the average accuracy (the *PCC*) and the average *Kappa* coefficient and δ of the random noise, respectively, for the proposed method.

TABLE IX
AVERAGE PERFORMANCE MEASURES FOR THE EXPERIMENT DATA.

| Dataset | Method | $\overline{FN}$ | $\overline{FP}$ | $\overline{OE}$ | $\overline{PCC}$ | $\overline{Kappa}$ | $\overline{F1-score}$ | $\overline{T(s)}$ |
|---|---|---|---|---|---|---|---|---|
| Average | PCANET | 0 | 4679.4 | 4679.4 | 0.9286 | 0.1466 | 0.1496 | 1097 |
| | NSST | 5 | 588.3 | 593.3 | 0.9910 | 0.4217 | 0.4235 | 2.75 |
| | NR_ELM | 15.5 | 700.6 | 716.1 | 0.9891 | 0.3548 | 0.3567 | 8.41 |
| | PCA_KMEANS | 19.6 | 2319.9 | 2339.5 | 0.9643 | 0.6280 | 0.6291 | **0.54** |
| | CWNN | 41.8 | 3076.3 | 3118.1 | 0.9524 | 0.3443 | 0.3461 | 12.17 |
| | PROPOSED | 17.1 | 4.9 | 22 | **0.9997** | **0.9028** | **0.9030** | 0.59 |

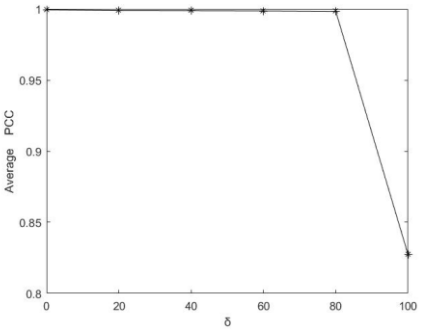


**FIGURE 13. The relationship between the average accuracy (PCC) of the proposed method and the standard deviation δ of random noise.**

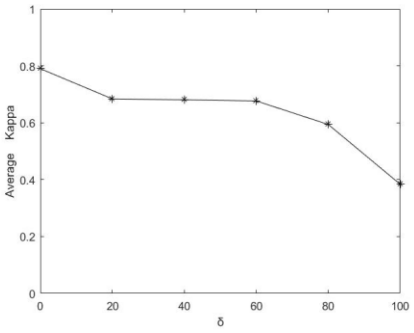


**FIGURE 14. The relationship between the average Kappa coefficient of the proposed method and the standard deviation δ of random noise.**

## V. CONCLUSION

The objective of this study is to reduce the effect of sensor noise on change detection in monitored images and decrease the run time of the change detection algorithm. We proposed a novel multitemporal monitoring image change detection algorithm based on morphological structure filtering and normalized fusion difference image. First, the random noise in two multitemporal monitoring images was removed by a multidirectional weighted multiscale series structure filter. Next, two difference images were obtained by using a compression log-ratio operator and a mean ratio operator respectively, and a fusion difference image was generated by simple equal weight fusion. The residual noise in two monitoring images was further removed, while the details of the changed area were retained. When the scene reflected by the two multitemporal monitoring images does not change, the difference in the sensor noise between the multitemporal monitoring images is obvious. We used the sigmoid function to normalize the fusion difference map, thereby suppressing the sensor noise between the two images and improving the subsequent clustering performance. Finally, the k-means clustering algorithm was utilized to obtain the change detection results. Subjective and objective evaluations of the experimental results demonstrate that the superiority of the proposed method over most popular reference algorithms in terms of change detection accuracy, time and robustness. Future work is planned to explore algorithms that encode changes in pixels over consecutive times as spikes and then

using a spiking neural network to detect the overall changes in the scene [39].

## REFERENCES

[1] Q. Yang, C. Jung, Q. Fu, and H. Song, "Low Light Image Denoising Based on Poisson Noise Model and Weighted TV Regularization," in *international conference on image processing*, 2018, pp. 3199-3203.

[2] M. Kim, D. Park, D. K. Han, and H. Ko, "A novel approach for denoising and enhancement of extremely low-light video," *IEEE Transactions on Consumer Electronics,* vol. 61, no. 1, pp. 72-80, 2015.

[3] M. Gong, Y. Cao, and Q. Wu, "A Neighborhood-Based Ratio Approach for Change Detection in SAR Images," *IEEE Geoscience and Remote Sensing Letters,* vol. 9, no. 2, pp. 307-311, 2012.

[4] G. Gao, X. Wang, M. Niu, and S. Zhou, "Modified log-ratio operator for change detection of synthetic aperture radar targets in forest concealment," *Journal of Applied Remote Sensing,* vol. 8, no. 1, pp. 083583-083583, 2014.

[5] J. Inglada and G. Mercier, "A New Statistical Similarity Measure for Change Detection in Multitemporal SAR Images and Its Extension to Multiscale Change Analysis," *IEEE Transactions on Geoscience and Remote Sensing,* vol. 45, no. 5, pp. 1432-1445, 2007.

[6] F. Gao, J. Dong, B. Li, Q. Xu, and C. Xie, "Change detection from synthetic aperture radar images based on neighborhood-based ratio and extreme learning machine," *Journal of Applied Remote Sensing,* vol. 10, no. 4, pp. 046019-046019, 2016.

[7] B. Hou, Q. Wei, Y. Zheng, and S. Wang, "Unsupervised Change Detection in SAR Image Based on Gauss-Log Ratio Image Fusion and Compressed Projection," *IEEE Journal of Selected Topics in Applied Earth Observations and Remote Sensing,* vol. 7, no. 8, pp. 3297-3317, 2014.

[8] M. Gong, Z. Zhou, and J. Ma, "Change Detection in Synthetic Aperture Radar Images based on Image Fusion and Fuzzy Clustering," *IEEE Transactions on Image Processing,* vol. 21, no. 4, pp. 2141-2151, 2012.

[9] L. Qingsong, Q. Xizhong, J. Zhenhong, Y. Jie, and H. Yingjie, "An unsupervised change detection of SAR images based on NSCT and FCM Clustering," *Laser Journal,* vol. 34, no. 4, pp. 20-22, 2013.

[10] H. Zhuang, K. Deng, Y. Yu, and H. Fan, "An approach based on discrete wavelet transform to unsupervised change detection in multispectral images," *International Journal of Remote Sensing,* vol. 38, no. 17, pp. 4914-4930, 2017.

[11] Z. Wenyan, J. Zhenhong, Y. Yu, J. Yang, and N. Kasabov, "SAR image change detection based on equal weight image fusion and adaptive threshold in the NSST domain," *European Journal of Remote Sensing,* vol. 51, no. 1, pp. 785-794, 2018.

[12] T. Celik, "Unsupervised Change Detection in Satellite Images Using Principal Component Analysis and $k$-Means Clustering," *IEEE Geoscience and Remote Sensing Letters,* vol. 6, no. 4, pp. 772-776, 2009.

[13] J. B. Collins and C. E. Woodcock, "An assessment of several linear change detection techniques for mapping forest mortality using multitemporal landsat TM data," *Remote Sensing of Environment,* vol. 56, no. 1, pp. 66-77, 1996.

[14] Y. Wang, L. Du, and H. Dai, "Unsupervised SAR Image Change Detection Based on SIFT Keypoints and Region Information," *IEEE Geoscience and Remote Sensing Letters,* vol. 13, no. 7, pp. 931-935, 2016.

[15] R. Shang, Y. Yuan, L. Jiao, Y. Meng, and A. M. Ghalamzan, "A self-paced learning algorithm for change detection in synthetic aperture radar images☆," *Signal Processing,* vol. 142, pp. 375-387, 2018.

[16] F. Gao, J. Dong, B. Li, and Q. Xu, "Automatic Change Detection in Synthetic Aperture Radar Images Based on PCANet," *IEEE Geoscience and Remote Sensing Letters,* vol. 13, no. 12, pp. 1792-1796, 2016.

[17] F. Gao, X. Wang, Y. Gao, J. Dong, and S. Wang, "Sea Ice Change Detection in SAR Images Based on Convolutional-Wavelet Neural Networks," *IEEE Geoscience and Remote Sensing Letters,* vol. 16, no. 8, pp. 1240-1244, 2019.

[18] Y. Zheng, L. Jiao, H. Liu, X. Zhang, B. Hou, and S. Wang, "Unsupervised saliency-guided SAR image change detection," *Pattern Recognition,* vol. 61, no. 61, pp. 309-326, 2017.

[19] Y. Zhang, S. Wang, C. Wang, J. Li, and H. Zhang, "SAR Image Change Detection Using Saliency Extraction and Shearlet Transform," *IEEE Journal of Selected Topics in Applied Earth Observations and Remote Sensing,* vol. 11, no. 12, pp. 4701-4710, 2018.

[20] S. Roth and M. J. Black, "Fields of Experts: a framework for learning image priors," in *computer vision and pattern recognition*, 2005, vol. 2, pp. 860-867.

[21] A. Buades, B. Coll, and J. Morel, "A non-local algorithm for image denoising," in *computer vision and pattern recognition*, 2005, vol. 2, no. 2, pp. 60-65.

[22] W. Dong, L. Zhang, G. Shi, and X. Li, "Nonlocally Centralized Sparse Representation for Image Restoration," *IEEE Transactions on Image Processing,* vol. 22, no. 4, pp. 1620-1630, 2013.

[23] H. Li and F. Liu, "Image Denoising Via Sparse and Redundant Representations Over Learned Dictionaries in Wavelet Domain," in *international conference on image and graphics*, 2009, pp. 754-758.

[24] J. Mairal, F. Bach, J. Ponce, G. Sapiro, and A. Zisserman, "Non-local sparse models for image restoration," in *international conference on computer vision*, 2009, pp. 2272-2279.

[25] K. Dabov, A. Foi, V. Katkovnik, and K. Egiazarian, "Image Denoising by Sparse 3-D Transform-Domain Collaborative Filtering," *IEEE Transactions on Image Processing,* vol. 16, no. 8, pp. 2080-2095, 2007.

[26] P. Lin, B. Chen, F. Cheng, and S. Huang, "A Morphological Mean Filter for Impulse Noise Removal," *IEEE/OSA Journal of Display Technology,* vol. 12, no. 4, pp. 344-350, 2015.

[27] L. Liu, Z. Jia, J. Yang, and N. Kasabov, "SAR Image Change Detection Based on Mathematical Morphology and the K-Means Clustering Algorithm," *IEEE Access,* vol. 7, pp. 43970-43978, 2019.

[28] X. Li, L. Wang, J. Wang, and X. Zhang, "Multi-focus image fusion algorithm based on multilevel morphological component analysis and support vector machine," *Iet Image Processing,* vol. 11, no. 10, pp. 919-926, 2017.

[29] H. Shih and E. Liu, "Automatic Reference Color Selection for Adaptive Mathematical Morphology and Application in Image Segmentation," *IEEE Transactions on Image Processing,* vol. 25, no. 10, pp. 4665-4676, 2016.

[30] W. Huang, R. Wang, Y. Zhou, and X. Chen, "Simultaneous Coherent and Random Noise Attenuation by Morphological Filtering With Dual-Directional Structuring Element," *IEEE Geoscience and Remote Sensing Letters,* vol. 14, no. 10, pp. 1720-1724, 2017.

[31] F. G. B. De Natale and G. Boato, "Detecting Morphological Filtering of Binary Images," *IEEE Transactions on Information Forensics and Security,* vol. 12, no. 5, pp. 1207-1217, 2017.

[32] L. Hu, C. Qi, S. Chen, and Q. Wang, "An Improved Heuristic Optimization Algorithm for Feature Learning Based on Morphological Filtering and its Application," *IEEE Access,* vol. 6, pp. 22754-22763, 2018.

[33] J. Ma, M. Gong, and Z. Zhou, "Wavelet Fusion on Ratio Images for Change Detection in SAR Images," *IEEE Geoscience and Remote Sensing Letters,* vol. 9, no. 6, pp. 1122-1126, 2012.

[34] W. Ma, X. Li, Y. Wu, L. Jiao, and D. Xing, "Data Fusion and Fuzzy Clustering on Ratio Images for Change Detection in Synthetic Aperture Radar Images," *Mathematical Problems in Engineering,* vol. 2014, pp. 1-14, 2014.

[35] S. Patra, S. Ghosh, and A. Ghosh, "Histogram thresholding for unsupervised change detection of remote sensing images," *International Journal of Remote Sensing,* vol. 32, no. 21, pp. 6071-6089, 2011.

[36] N. S. Mishra, S. Ghosh, and A. Ghosh, "Fuzzy clustering algorithms incorporating local information for change detection

in remotely sensed images," *Applied Soft Computing,* vol. 12, no. 8, pp. 2683-2692, 2012.

[37] P. L. Rosin and E. Ioannidis, "Evaluation of global image thresholding for change detection," *Pattern Recognition Letters,* vol. 24, no. 14, pp. 2345-2356, 2003.

[38] G. H. Rosenfield and K. Fitzpatricklins, "A coefficient of agreement as a measure of thematic classification accuracy," *Photogrammetric Engineering and Remote Sensing,* vol. 52, no. 2, pp. 223-227, 1986.

[39] N. K. Kasabov, "[Springer Series on Bio- and Neurosystems] Time-Space, Spiking Neural Networks and Brain-Inspired Artificial Intelligence Volume 7 || Evolving Spiking Neural Networks," vol. 10.1007/978-3-662-57715-8, no. Chapter 5, pp. 169-199, 2019.

**Yong Zhu** received a bachelor's degree in electronic information engineering from school of information science and engineering, Anhui University of architecture, China in 2018. From 2018 to 2021, he obtained a master's degree from the school of information science and engineering, Xinjiang University, China.

His research direction is image change detection.

**Zhen-Hong Jia** received the B.S.degree in Beijing Normal University, Beijing, China, in 1985 and 1987. And the M.S.degree and the Ph.D. degree from Shanghai Jiao Tong University, Shanghai, China, in 1987 and 1995. Currently, he is a professor at the Autonomous University Key Laboratory of signal and information processing laboratory, Xinjiang University, China.

His research interests include digital image processing, Photoelectric information detection and sensor.

**Jie Yang** received his PhD from the Department of Computer Science, Hamburg University, Germany, in 1994. Currently, he is a professor at the Institute of Image Processing and Pattern Recognition, Shanghai JiaoTong University, China.

His major research interests are object detection and recognition, data fusion and data mining, and medical image processing.

**NIKOLA K. KASABOV**(M'93–SM'98–F'10) received the M.S. degree in computing and electrical engineering and the Ph.D. degree in mathematical sciences from the Technical University of Sofia, Sofia, Bulgaria, in 1971 and 1975, respectively. He is currently the Director and the Founder of the Knowledge Engineering and Discovery Research Institute and a Professor of knowledge engineering with the School of Computing and Mathematical Sciences, Auckland University of Technology, Auckland, New Zealand.

His major research interests include information science, computational intelligence, neural networks, bioinformatics, neuroinformatics, speech and image processing in which areas he has published more than 650 works.